LASER & PHOTONICS REVIEWS
www.lpr-journal.org

Photonic Bound States in the Continuum in Si Structures with the Self-Assembled Ge Nanoislands

Sergey A. Dyakov, Margarita V. Stepikhova, Andrey A. Bogdanov, Alexey V. Novikov, Dmitry V. Yurasov, Mikhail V. Shaleev, Zakhary F. Krasilnik, Sergei G. Tikhodeev, and Nikolay A. Gippius*

Germanium self-assembled nanoislands and quantum dots are very prospective for CMOS-compatible optoelectronic integrated circuits but their photoluminescence (PL) intensity is still insufficient for many practical applications. Here, it is demonstrated experimentally that the PL of Ge nanoislands in silicon photonic crystal slabs (PCS) with hexagonal lattice can be dramatically enhanced due to the involvement in the emission process of the bounds states in the continuum. These high-Q photonic resonances allow to achieve PL resonant peaks with the quality factor as high as 2200 and with the peak PL enhancement factor of more than two orders of magnitude. The corresponding integrated PL enhancement is demonstrated to be more than one order of magnitude. This effect is studied theoretically by the Fourier modal method in the scattering matrix form. The symmetry of the quasi-normal guided modes in the PCS is described in terms of group theory. This work paves the way toward a new class of optoelectronic components compatible with silicon technology.

1. Introduction

Silicon technology is the base of modern nanoelectronics. In spite of active search of an alternative platform like plasmonics, polaritonics, graphene electronics„ it is hard to imagine that some of them can replace silicon technology in the nearest future. One of the main challenges of silicon photonics is a lack of effective light sources that can be incorporated in CMOS-compatible integrated circuits. A plethora of possible candidates for active media in silicon photonics was analyzed in detail for the last four decades.

In particular, much attention was paid to Er-doped silicon structures giving luminescence peak around 1.55 μm.[1,2] However, due to a rather long spontaneous transition lifetime and the limited solid solubility of Er in Si, photoluminescence efficiency is quite low.[3–5] Another prospective active medium compatible with silicon technology is n-Ge strained layers giving luminescence in the telecommunication spectral range. Application of tensile strain and/or heavy n-type doping can effectively reduce the energy difference between the direct and indirect transitions in Ge increasing the probability of radiative recombination.[6] Using heavy doping and low strain lasing in Ge was demonstrated both under optical[7] and electrical[8] pumping. However, the thresholds were unpractically large. Subsequent application of higher strains allowed to achieve laser action at much smaller thresholds but at cryogenic temperatures.[9–11]

Direct-bandgap transitions can be achieved in GeSn alloys offering a tunable bandstructure.[12–17] Luminescence can be also obtained from Si itself due to the quantum confinement spreading out the carrier wavefunction in the momentum space increasing the probability of radiative processes. Such a luminescence was demonstrated in porous Si,[18,19] Si nanocrystals,[20–24] and Si/Ge quantum wells.[25] Light-emitting A_3B_5 structures can be integrated to silicon platform via direct epitaxial growth[26–29] or wafer bonding techniques.[30–32] In spite of intensive study, none of the named above luminescence mechanisms found large-scale implementation in industry.

An alternative CMOS-compatible active medium is Ge self-assembled nanoislands. Room-temperature photoluminescence (PL) is observed in such structures at wavelengths 1.3–1.6 μm

Dr. S. A. Dyakov, Prof. N. A. Gippius
Center of Photonics and Quantum Materials
Skolkovo Institute of Science and Technology
Nobel Street 3, Moscow 143026, Russia
E-mail: s.dyakov@skoltech.ru
Dr. M. V. Stepikhova, Dr. A. V. Novikov, Dr. D. V. Yurasov, Dr. M. V. Shaleev, Prof. Z. F. Krasilnik
Department of Semiconductor Physics
Institute for Physics of Microstructures RAS
GSP-105, Nizhny Novgorod 603950, Russia
Dr. A. V. Novikov, Prof. Z. F. Krasilnik
Faculty of Radiophysics
Lobachevsky State University of Nizhny Novgorod
Gagarin Ave. 23, Nizhny Novgorod 603950, Russia
Prof. A. A. Bogdanov
Department of Physics and Engineering
ITMO University
Birjevaja Line V.O. 14, St. Petersburg 199034, Russia
Prof. S. G. Tikhodeev
Faculty of Physics
Lomonosov Moscow State University
Leninskie Gory, GSP-1, Moscow 119991, Russia
Prof. S. G. Tikhodeev
A.M. Prokhorov General Physics Institute
Vavilova St. 38, Moscow117942, Russia
The ORCID identification number(s) for the author(s) of this article can be found under https://doi.org/10.1002/lpor.202000242

DOI: 10.1002/lpor.202000242

(0.75–0.95 eV). However, due to the spatial separation of holes and electrons in Ge nanoislands,[33] their radiative recombination efficiency is not high enough for practical applications. There are several approaches for the increase of this efficiency among which may be mentioned a vertical arrangement of nanoislands in a lattice[34] and ion bombarding of Ge nanoislands.[35] Thus, the low-temperature laser generation was demonstrated in whispering gallery mode resonators with built-in Ge nanoislands.[35]

Photoluminescence from Ge nanoislands can be enhanced via the Purcell effect in various resonant photonic structures including Mie resonators,[36] photonic crystal cavities,[37,38] metasurfaces,[39,40] nanoantennas.[39] An important advantage of Ge nanoislands is that they can be precisely positioned at the hotspots of the mode in photonic structures.[41] Photonic crystal cavities demonstrate extremely high Q/V values and, thus, high Purcell factor offering a lot of benefits for compact optical devices with strong light–matter interaction.[42,43] From the other side, due to a small active region of photonic crystal cavities in comparison with the overall footprint, they are not very promising for light-emitting applications.

Periodic photonic structures without cavities can support high-Q states with a mode profile homogeneously spread over the whole photonic structure. Such states are now called bound states in the continuum (BICs) and they have recently attracted enormous attention in photonics.[44–63] BICs represent spatially localized states with vanishing radiation despite their energy embedded in the continuum spectrum of the environment. Fundamentally, BICs originate from destructive interference, when two or more waves superpose to completely suppress radiative losses.[61,64–66] Therefore, their radiative quality (Q) factor diverges in theory. However, in practice, due to the finite size of the sample, roughnesses, and other imperfections, the radiative Q factor of BIC becomes finite but extremely large.[67–69] BICs were first predicted in quantum mechanics around a century ago[70] but in optics, they have been actively studied over the last decade.[71–74] The close attention paid to BICs is explained by a variety of their potential applications for resonant field enhancement,[75,76] lasing,[77–79] filtering of light,[80,81] sensing,[82–84] enhancement of light–matter interaction,[85,86] polarization control,[87,88] and nonlinear photonics.[89–93] The mechanism resulting in the appearance of BIC in periodic structures can be exploited to engineer high-Q states (quasi-BIC) in single resonators.[94–97]

In spite of more than 20 years history of BICs, these resonances have been mostly considered in z-symmetrical structures with a square photonic crystal lattice. Although hexagonal lattices are more often used for design of high-Q photonic crystal cavities and for grating-assisted coupling of the far field with the near field,[98–100] they have received much less attention by the BIC community. Especially it concerns the practical demonstration of BIC-originated enhancement of photoluminescence (PL) from hexagonal photonic crystal slabs (PCSs).

In this work we study the BIC-originated PL enhancement of Ge self-assembled nanoislands embedded in PCS with hexagonal lattice. Here, in contrast to previous publications, we employ not only a singlet BIC, a common property of both square and hexagonal lattices, but also a doublet BIC, a unique feature of C_{6v} symmetric structures. We experimentally demonstrate that due to the BICs in our PCS, we manage to achieve photoluminescence resonant peaks with the quality factor of 2200 as well as more than two orders of magnitude peak photoluminescence enhancement and more than one order of magnitude integrated PL enhancement compared with the nonstructured sample area. We attribute the observed photoluminescence peaks to quasiguided modes of the PCS and describe their symmetry in terms of irreducible representations of the C_{6v} point group. We also explain why different BICs are seen in the photoluminescence spectra as peaks, although it is broadly believed that BICs should be optically inactive.

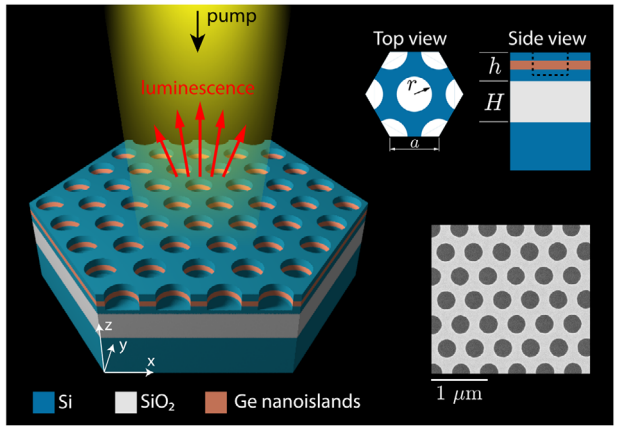

Figure 1. Schematics of the PCS with five layers of Ge nanoislands. Insets show the top and side views of the PCS and the SEM image of the PCS with air pores in Si matrix.

2. PL Enhancement and Quasiguided Modes

To study the effect of the PL enhancement we use the PCS with hexagonal photonic crystal lattice of air pores (**Figure 1**) formed in structures with Ge self-assembled nanoislands grown by molecular beam epitaxy on SOI wafer with the thickness of buried oxide $H = 3$ μm. The thickness of the whole structure above the buried oxide was $h = 300$ nm, which included the 60 nm thick Ge nanoislands lattice consisting of 5 layers with Ge nanoislands separated by 15 nm Si spacer layers. Such lattice was sandwiched between the 75 and 165 nm thick capping and buffer Si layers, respectively. The lattice period of a photonic crystal, a, was varied in the range from 450 to 725 nm, and the ratio of the pore radius to period was $r/a = 0.2$ and 0.26. We measure the PL spectra of the PCSs using two different schemes, namely, the microphotoluminescence (μPL) and directional photoluminescence (DPL) schemes. The main difference between them is the solid angle to the surface normal from which the PL signal is detected (see Experimental Section).

Experimental PL spectra measured with DPL technique (collection angle ±6° to the surface normal) at room temperature for PCS with different periods are shown in **Figure 2**. One can see that each PL spectrum from PCS consists of several resonance peaks. The experimental peaks have the following features: i) there are narrow and wide peaks; ii) some of the peaks have a fine structure; iii) peaks have a profile which is close to a Laurentian. The peaks spectral position redshifts with an increase of the lattice period. It is well known that PCSs have

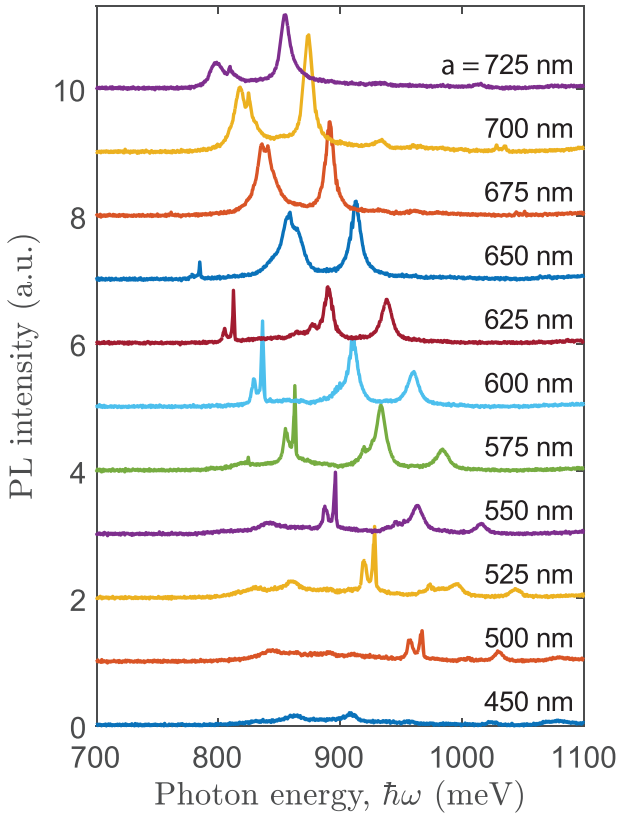

Figure 2. Experimental PL spectra for different photonic crystal periods measured at room temperature in DPL scheme. For all spectra $r/a = 0.2$.

such peaks in their optical spectra of reflection, transmission, and photoluminescence.[101,102] They represent the quasiguided modes,[101] (also known as quasi-normal guided modes[103,104]) that appear due to the grating-assisted coupling of waveguide modes with photon continuum of the far field. To establish the cause of differences in the peaks, below we study the nature and symmetry of the modes of our hexagonal lattice in detail.

We start from the empty lattice approximation and plot the resonances of the effective homogeneous waveguide folded into the first Brillouin zone of the hexagonal lattice (**Figure 3**a). In the displayed spectral range, one can observe several families of modes in the Γ-point. They correspond to the TE_1 and TM_1 waveguide modes (blue and red curves, respectively) and the TE_2 mode (green curve). With the introduction of the pores, these modes start to interact with each other which results in splitting and bending of their dispersion curves. This is illustrated in Figure 3b, where we present the calculated photon energy, $\hbar\omega$, and in-plane wavevector, $k_{\|}$, the dependence of the emissivity of a hypothetical low-contrast (weak) grating where the dielectric permittivity of the substance in pores is only 20% less than the dielectric permittivity of the matrix. One can see that in the weak grating the modes in Γ-point are split, but the dispersions of quasiguided modes can be described roughly in the empty lattice approximation. The number of the first-order quasiguided modes in the hexagonal photonic crystal lattice is 12, although not all of them can be distinguished in the dispersion diagram in Figure 3b as some of them are still too close to each other. One can see in Figure 3b that in the Γ-point some of the modes are degenerate while out of the Γ-point the degeneracy is lifted. The group theory predicts for our C_{6v} symmetric hexagonal PCS that in the Γ-point there are doubly degenerate modes (i.e., doublets) and nondegenerate modes (i.e., singlets). The number of singlets and doublets is determined by a symmetry of the photonic crystal lattice. Here there are four first-order singlets and four first-order doublets. With the increase of the grating contrast, the modes continue to hybridize forming an even more complicated dispersion diagram (Figure 3c). However, the number of modes and their degree of degeneracy in the Γ-point remain unchanged.

Since all the resonances have a dispersion with $k_{\|}$, the resonance peaks, which appear in the measured PL spectra, inhomogeneously broaden due to a nonzero numerical aperture (NA) of the collecting lens. One can reduce the effect of such aperture by using the lens with a smaller NA. This can be understood by inspecting Figure 3c where the green and magenta lines bound 6° and 25° light cones from which the PL light is collected in our DPL and μPL setups, respectively (see Experimental Section). The corresponding experimental PL spectra for PCS with $a = 570$ nm and $r/a = 0.26$ are shown in Figure 3d. One can see from the presented spectra that the position of the resonance peaks coincides quite well with the calculated position of the modes near the Γ-point in Figure 3c. When the PL is measured from inside the 25° cone, the resonance peak positions are averaged over the wide range of emission angles. It leads to a stronger integrated PL signal and broader resonance peaks. The resulting PL intensity of the PCS is enhanced by a factor of $f_{max} = 140$ at $\hbar\omega = 932$ meV (1330 nm) compared to the PL intensity of the nonprocessed film. The spectrally integrated enhancement factor is $f_{int} = 13$. Whereas the PL spectra measured from inside the 6° cone have a weaker PL intensity but narrower peaks. Moreover, the peak positions in the DPL spectra correspond more closely to the calculated PCS quasiguided modes in the Γ-point.

Let us consider the emissivity dispersion diagrams near the Γ-point calculated for different photonic crystal periods, namely $a = 525$ nm, $a = 600$ nm and $a = 675$ nm (**Figure 4**a–c). With an increase of a the first Brillouin zone decreases and, as can be seen from Figure 4a–c, the spectral position of quasiguided modes redshifts. As a result, for different photonic crystal periods, different modes fall into the Ge nanoislands intrinsic emission range, bounded by the blue lines in Figure 4a–c. This is in agreement with the experimental spectra shown in Figure 2 where some of the modes become invisible with an increase of a. Although there is a quite good match between the energy position of theoretically calculated modes and experimentally measured PL peaks (Figure 4), some resonances manifest themselves in the measured PL spectra better than others. This is due to the fact that some of the resonances have almost a flat dispersion within 6 ° collecting cone, for example, the upper E_1 mode, while others have stronger dispersion such as the B_1 mode (the explanation of the formalism of the modes designation will be given later).

As has been mentioned above, the PL spectra of different PCSs have resonant peaks of different widths. This can be seen from the detailed spectra for PCSs with $a = 525$ nm, $a = 600$ nm, and $a = 675$ nm shown separately in Figure 4d–f. The experimental Q-factor of the peaks estimated as $Q = \lambda/\Delta\lambda$ is between 150 and 2200. To the best of our knowledge, the achieved Q-factor of 2200 is the highest Q-factor value in spontaneous emission

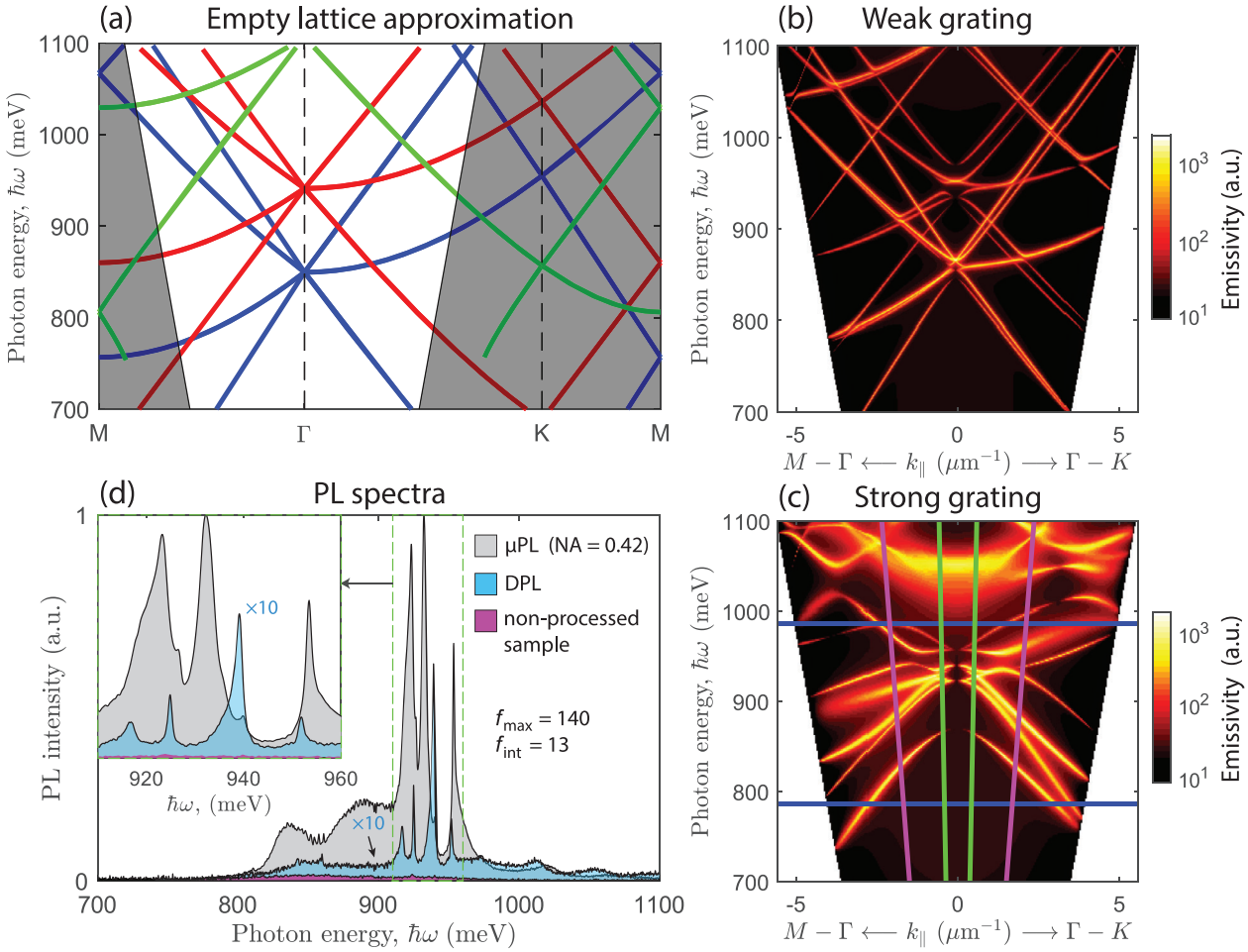

Figure 3. a) Dispersion of the quasiguided modes of the PCS in empty lattice approximation with PCS period $a = 570$ nm. Blue, red, and green colors denote, respectively, TE_1, TM_1, and TE_2 quasiguided modes. Gray color denotes the region below the vacuum light line. b,-c) Photon energy and in-plane wavevector dependence of emissivity calculated for weak and strong gratings with $a = 570$ nm and $r/a = 0.26$. Green and magenta lines in panel (c) denote the 6° and 25° light cones from which the PL light is collected in DPL and μPL techniques, respectively. Blue lines bound the energy range of intrinsic photoluminescence of Ge nanoislands. Maps in panels (b) and (c) are presented in the logarithmic color scale shown on the right. d) PL spectra measured for the PCS with $a = 570$ nm and $r/a = 0.26$ using μPL and DPL techniques. Inset in (d) shows the same spectra on an enlarged scale. The peak μPL enhancement is $f_{max} = 140$, integral μPL enhancement is $f_{int} = 13$.

up to now after Refs. [79, 105] where the lasing regimes are considered. Please note that Q-factors of quasiguided modes in photonic crystals slabs measured in transmission or reflection modes[82,84,106–124] are generally higher than those measured in emission mode[58,79,105,125–128] due to the inevitable absorption in the luminescent materials.

We now focus on the differences of the Q-factors of different PL resonant peaks. In order to explain these differences, the symmetry of quasiguided modes has to be considered.

3. Symmetry of Modes

The spatial symmetry of the quasiguided modes plays an important role in their optical response. The symmetry is determined by the type of the photonic crystal lattice and can be classified in terms of the group theory.[129,130] To study the symmetry of the modes in our PCS, we find the poles of the scattering matrix by solving the eigenvalue problem (see Experimental Section for details.). In the case of doublets, the solution is represented by the basis of two eigenfunctions; any linear combination of these eigenfunctions is a solution of the eigenvalue problem too. This fact gives the essential advantage to the doublet modes over singlet ones in structures with randomly placed quantum emitters (like QDs or nanoislands). Indeed, the field distribution for singlet modes is predefined in contrast to the case of doublet modes and a Ge nanoisland near the node of a singlet mode cannot couple efficiently to it. But for doublet modes by virtue of their degeneracy, the field profile will be self-adjusted to provide the maximal overlap integral with randomly placed emitters. A similar thing happens in microdisk resonators hosting whispering gallery modes which are degenerate due to the rotational symmetry (clockwise and contra-clockwise modes).[131,132]

The spatial distributions of intensity and z-component of the electric field found from the output eigenvectors $|\mathbf{O}\rangle_{res}$ are shown in **Figure 5**a,b for the Γ-point. One can see that the intensity distributions in singlets are C_{6v} symmetrical following the

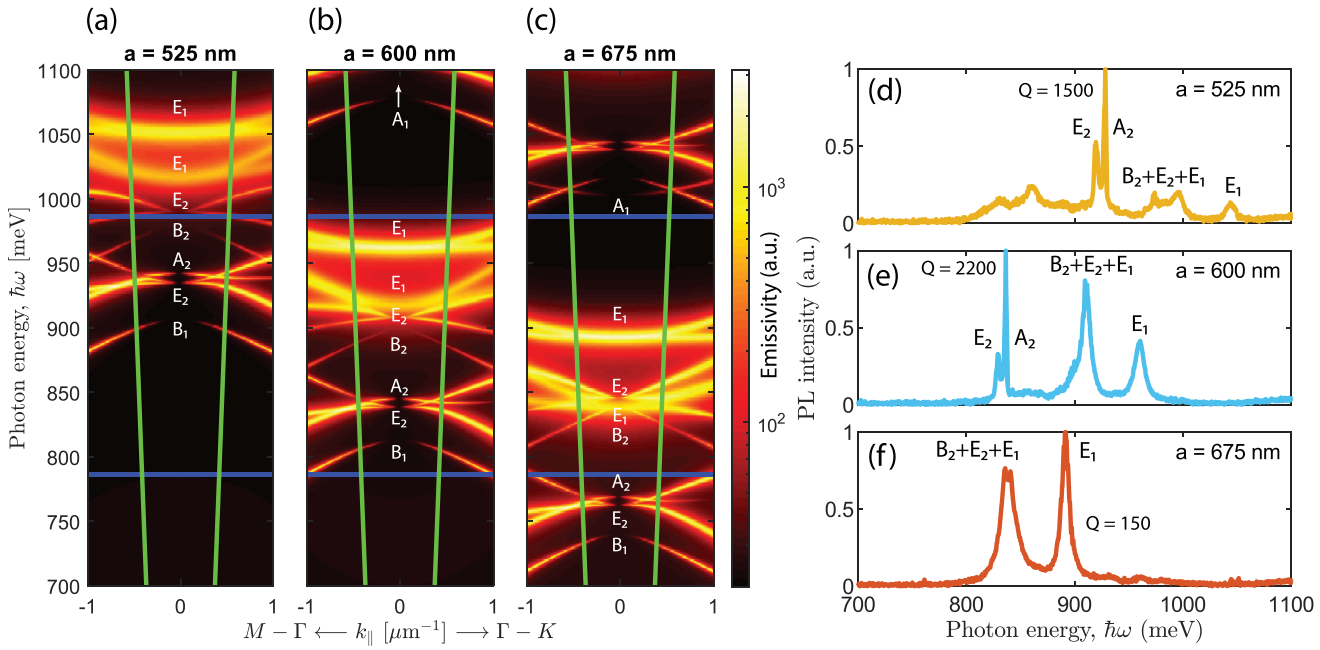

Figure 4. a–c) Calculated emissivity near Γ-point at $r/a = 0.2$ for different photonic crystal periods. The logarithmic color scale shown on the right. Green lines denote the 6° light cone from which the PL light is collected. Horizontal blue lines bound the energy range of intrinsic photoluminescence of Ge nanoislands. d–f) Experimental PL spectra measured in the DPL scheme for different photonic crystal periods.

Table 1. Character table for C_{6v} point group.

	E	$2C_6$	$2C_3$	C_2	$3\sigma_y$	$3\sigma_x$
A_1	1	1	1	1	1	1
A_2	1	1	1	1	−1	−1
B_1	1	−1	1	−1	1	−1
B_2	1	−1	1	−1	−1	1
E_1	2	1	−1	−2	0	0
E_2	2	−1	−1	2	0	0

symmetry of the PCS. In the case of doublets, the intensity profile in the eigenmodes cannot be C_{6v} symmetrical, however, one can choose a basis of eigenfunctions such that the field intensities in them have a C_6 symmetry as shown in Figure 5a. The field intensities of two eigenfunctions are mirror symmetrical to each other by a vertical plane, that indicates the degeneracy of these modes. The E_z distributions in the singlets and doublets have more complex symmetries. The group theory defines symmetry of an eigenmode by a set of characters χ which characterize the mode transformation for each symmetry operation in the point group (see **Table 1**). By inspecting Figure 5b one can associate each of the field distributions E_z with a set of characters χ and, by this, determine to which irreducible representation of the C_{6v} point group they belong. In Figures 4 and 5, all 12 first-order quasiguided modes in the Γ-point are marked in accordance with the definitions in Table 1. Please note that the E_z distributions in both eigenfunctions of doublets are identical (bottom parts of Figure 5a,b).

Since the PCS under study has no horizontal plane of symmetry, its eigenmodes are not purely xy- or z-polarized. The intermediate polarization of such modes can be quantitatively described in terms of a two-component polarization measure C calculated as

$$C = \left(\frac{c_h}{c_h + c_v}, \frac{c_v}{c_h + c_v} \right) \tag{1}$$

where c_h and c_v are the values of the integrals over photonic crystal unit cell in real space

$$c_h = \int \left[|E_x(\vec{r})|^2 + |E_y(\vec{r})|^2 \right] d\vec{r} \tag{2}$$

$$c_v = \int |E_z(\vec{r})|^2 d\vec{r} \tag{3}$$

Polarization measures C calculated for different PCS eigenmodes are presented in **Table 2**. One can see from Table 2 that some of the modes have a predominant polarization (e.g., upper doublet E_1) while others do not have (e.g., lower doublet E_2). The predominant polarization of the eigenmodes does not explicitly determine whether horizontal or vertical oscillating dipoles give a major contribution to the overall PL intensity. See Supporting Information for more details.

To demonstrate that the local polarization of the eigenmodes can differ significantly from their predominant polarization, we present the phase distribution of electric field in the doublets E_1 and E_2 (Figure 5d) where the phase of electromagnetic oscillations is denoted by the color. Please see the details of this representation in Ref. [133] and the phase representation for other modes in Supporting Information. In Figure 5c,d one can simultaneously see that i) the presented field distributions

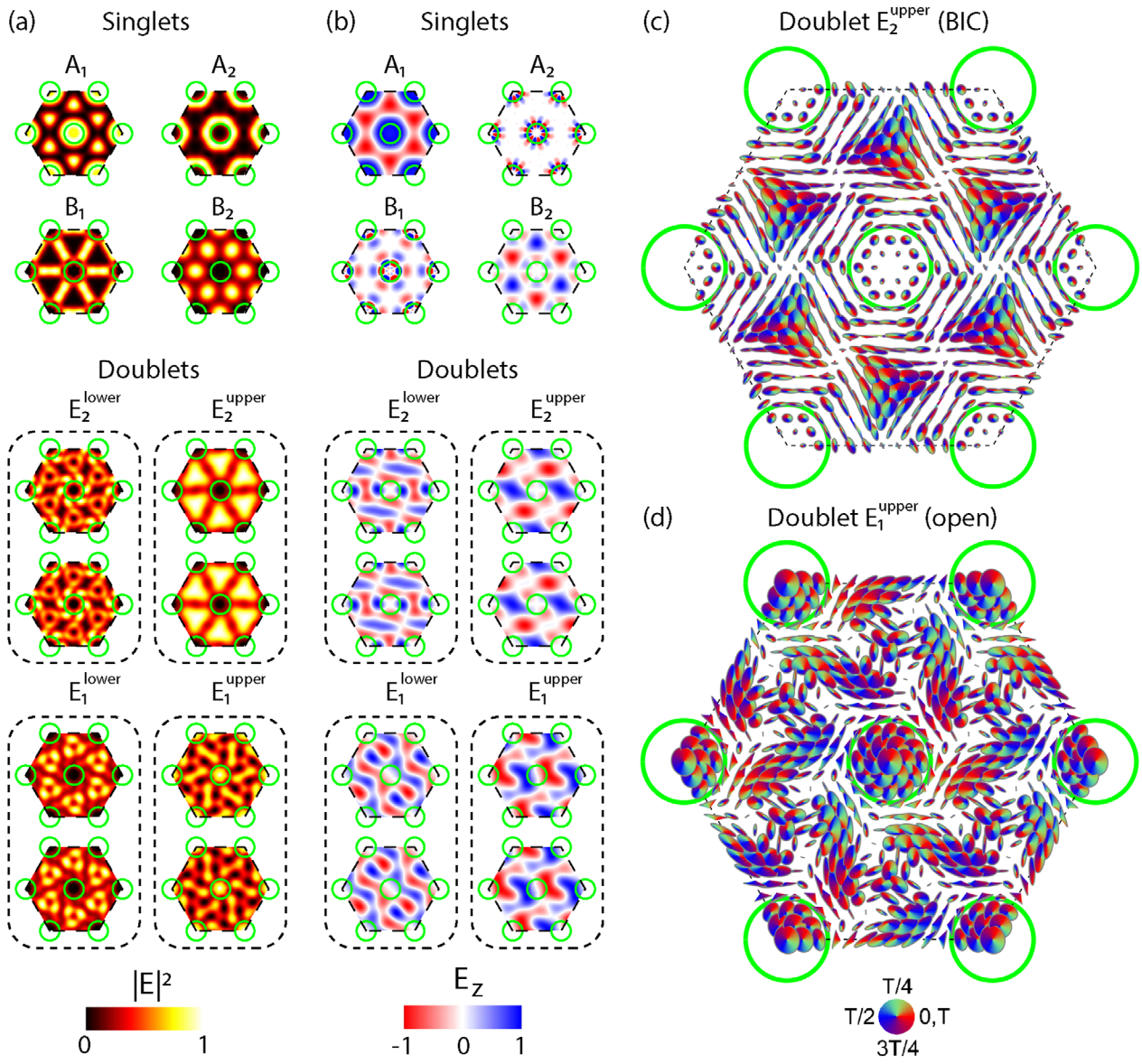

Figure 5. a) Electric field intensity and b) the real part of *z*-projection of electric vector in singlet and doublet eigenmodes of PCS with $a = 600$ nm, $r/a = 0.2$ calculated at *z*-coordinate in the middle of emitting layer. Photon energies of eigenmodes are the following: $\hbar\omega_{A_1} = 1088.3 - 0.705\text{i}$ meV, $\hbar\omega_{A_2} = 843.9 - 0.439\text{i}$ meV, $\hbar\omega_{B_1} = 812 - 0.458\text{i}$ meV, $\hbar\omega_{B_2} = 898.4 - 0.609\text{i}$ meV, $\hbar\omega_{E_1}^{\text{upper}} = 960.3 - 2.770\text{i}$ meV, $\hbar\omega_{E_1}^{\text{lower}} = 916.2 - 5.263\text{i}$ meV, $\hbar\omega_{E_2}^{\text{upper}} = 906.9 - 0.6\text{i}$ meV, $\hbar\omega_{E_2}^{\text{lower}} = 837.6 - 0.434\text{i}$ meV. Color scales for panels (a, -b) are shown at the bottom. Phase representation of electric field c) in the upper doublet E_2 and d) in the upper doublet E_1 for the PCS with $a = 600$ nm and $r/a = 0.2$. The phase of electromagnetic oscillations is represented by color as shown on the circular color chart. Please note that i) the cone base lies in the polarization plane where the field oscillates; ii) the cone height is equal to the product of the electric field amplitude and the circular polarization degree; iii) the direction of the cone follows the right screw rule.

are indeed the E_1 and E_2 modes; ii) the electric vectors are not linearly polarized; iii) the field intensity has C_6 rotational symmetry; iv) the field in the doublets E_2 and E_1 has nodes and antinodes in the centers of pores. The phase representation of the fields for the rest of the modes is shown in Supporting Information. Figure 5d shows only one of the two eigenfunctions of doublets E_1 and E_2. The second eigenfunction of each doublet is mirror symmetrical to the first eigenfunction with respect to a vertical plane passing through the centers of two nearest pores.

Understanding the symmetry of modes has a direct practical implication. Namely, it enables us to predict which modes can couple to the far field in the Γ-point. The coupling to free space is possible when the overlap integral γ is nonvanishing:

$$\gamma = \iint_{\text{cell}} \left(\vec{E}_{\text{fs}}^{*} \times \vec{H}_{\text{mode}} + \vec{E}_{\text{mode}}^{*} \times \vec{H}_{\text{fs}} \right) dS, \tag{4}$$

where dS is the element of the unit cell, indices fs and mode denote free space and modal electric and magnetic fields, E and H.

Table 2. Polarization measures C of the PCS eigenmodes calculated for the period $a = 600$ nm, $r/a = 0.2a$, $k_x = k_y = 0$. $C = (1,\ 0)$ corresponds to purely horizontal polarization, while $C = (0,\ 1)$ corresponds to purely vertical polarization.

Mode	Polarization measure
A_1	(0.167, 0.833)
A_2	(1.000, 0.000)
B_1	(0.973, 0.027)
B_2	(0.926, 0.074)
E_1 upper	(0.848, 0.152)
E_1 lower	(0.374, 0.626)
E_2 upper	(0.878, 0.122)
E_2 lower	(0.434, 0.566)

By analyzing the characters of irreducible representations of C_{6v} point group (Table 1) one can conclude that in the C_{6v} symmetrical hexagonal lattice only the doublet E_1 is open for the far-field coupling. Whereas all the singlets, as well as the doublet E_2 are closed. Such modes are referred to as symmetry-protected (SP) BICs.[45,134]

4. Bound States in the Continuum

As has been mentioned, the group theory tells us that the number of symmetry-protected BICs in a PCS is fixed and is defined by the type of the photonic crystal lattice. In the C_{6v} symmetrical hexagonal lattice, there are four types of singlet BICs and one type of doublet BICs irrespective of a particular geometry of the PCS. By variation of geometrical parameters, one can only change the spectral position of modes in the Γ-point. As BICs cannot couple to the far field, they do not have radiation losses and, hence, the imaginary part of their frequency should be strictly zero in structures without Ohmic losses. In practice, we always have small but inevitable radiation losses caused by imperfections of geometry, roughness, nonperiodicity, a limited number of periods in the PCS, etc. It results in the fact that the Q-factor of such modes is not infinite, however, it can be very large. Yet another reason for the suppression of the experimental Q-factor of the BICs is that they might be measured out of the Γ-point due to experimental constraints. As we move away from the Γ-point, the symmetry of the BICs is broken and, consequently, they become visible in the far field. This is the reason why in our experiment we observe the peaks which can be associated with the BIC modes.

To discuss this in more detail, we calculate the dispersions of the emissivity and the Frobenius norm of the scattering matrix in a narrow range of photon energy and in-plane wavevector near the modes A_2 and E_2 (**Figure 6**a,b). One can see that near the Γ-point the emissivity is suppressed as the modes A_2 and E_2 are the symmetry-protected BICs. Unlike the emissivity, the norm of the scattering matrix does not have similar discontinuities. Three local maxima at each $\vec{k}_{\|}$ represent the resonant poles; two of them degenerate in the Γ-point. The Q-factor of both of them in the Γ-point is extremely large as shown in Figure 6d,f. With an increase of $|k_{\|}|$ the degeneracy is lifted, and the Q-factor of A_2 and E_2 modes decreases. A similar in-plane wavevector dependence of the Q-factor can be observed for other BICs, as shown in Figure 6e for the singlet B_1 as an example. The Q-factor of the open doublet E_1 in the Γ-point is sufficiently smaller than that of the BICs (Figure 6c). This situation is experimentally demonstrated in Figures 2 and 4 where the peaks have different Q-factors.

One can see in Figure 6a,b that there is yet another point in k-space, besides Γ, where the emissivity is suppressed and the resonance has exactly vanishing width, namely $k_{\|} = 0.4\ \mu m^{-1}$ along the Γ-M direction. This is a BIC of Friedrich–Wintgen type[135] which is a result of destructive interference between the modes with similar radiation patterns in far field.[136] When two quasiguided modes pass each other as a function of the in-plane wavevector, the interference causes an avoided crossing of the resonances and for a given value of $k_{\|}$ one resonance has extremely large Q-factor and, hence, becomes a BIC.

As the emissivity of BICs in the Γ-point is strictly zero, it appears that the possibility to obtain the BIC-original peaks in the PL spectra depends on the Ohmic losses power and on the solid angle from where the PL signal is collected. To demonstrate this we calculate the $k_{\|}$ dependence of the peak emissivity near the singlet B_1 for different parameters n'' which models the Ohmic losses[137] and assumes some fixed density of Ge nanoislands (**Figure 7**a). The parameter n'' is the imaginary part of the effective refractive index of the layer with Ge nanoislands. This parameter has definitely to be proportional to the Ge nanoislands density, but it also grows with the degree of overall disorder, introduced into Ge layers. The estimate for our samples is $n'' = 0.01$ which we have used in calculations of Figures 3–5. One can see that for all n'' the peak emissivity rises with $|k_{\|}|$ reaching its maximum. With the increase of n'' the maximal peak emissivity moves away from the Γ-point. As a result, at $n'' = 0.01$, the total emissivity within the 6° light cone near the singlet B_1 is smaller than that near the dark doublet E_2 or bright doublet E_1, for instance (Figure 7b). It explains why the B_1 originated peak is poorly seen in the experimental DPL spectra unlike the other peaks (see Figure 4). It is remarkable that as long as the absorption losses are small ($n'' \leqslant 0.01$), the maximal peak emissivity is roughly proportional to n''. Hence, even at relatively high absorption (e.g., $n'' = 10^{-2}$), the peak PL becomes measurable provided that the PL signal is collected away of the Γ-point. Although, in the case of high absorption the quality factor of the resonance will be lower. Thus, in order to obtain high Q-factor resonance peaks one can use the advantage of BICs in lossless PCSs.

5. Conclusion

In conclusion, we have demonstrated experimentally that the photoluminescence of Ge nanoislands in silicon PCS with hexagonal lattice can be greatly enhanced by the symmetry-protected bounds states in the continuum. The quality factor of the photoluminescent peaks at some of the resonant frequencies was as high as 2200 and the peak enhancement factor reached 140, while the overall integrated PL intensity was increased by more an order of magnitude as well. In our PCS, the experimental PL peaks can be wide as well as narrow and exhibit sometimes a fine structure. We have theoretically simulated these spectral features by calculating the emissivity dispersion diagrams using the Fourier modal method (FMM) in the scattering matrix form. On the dispersion diagrams, we have shown the appearance

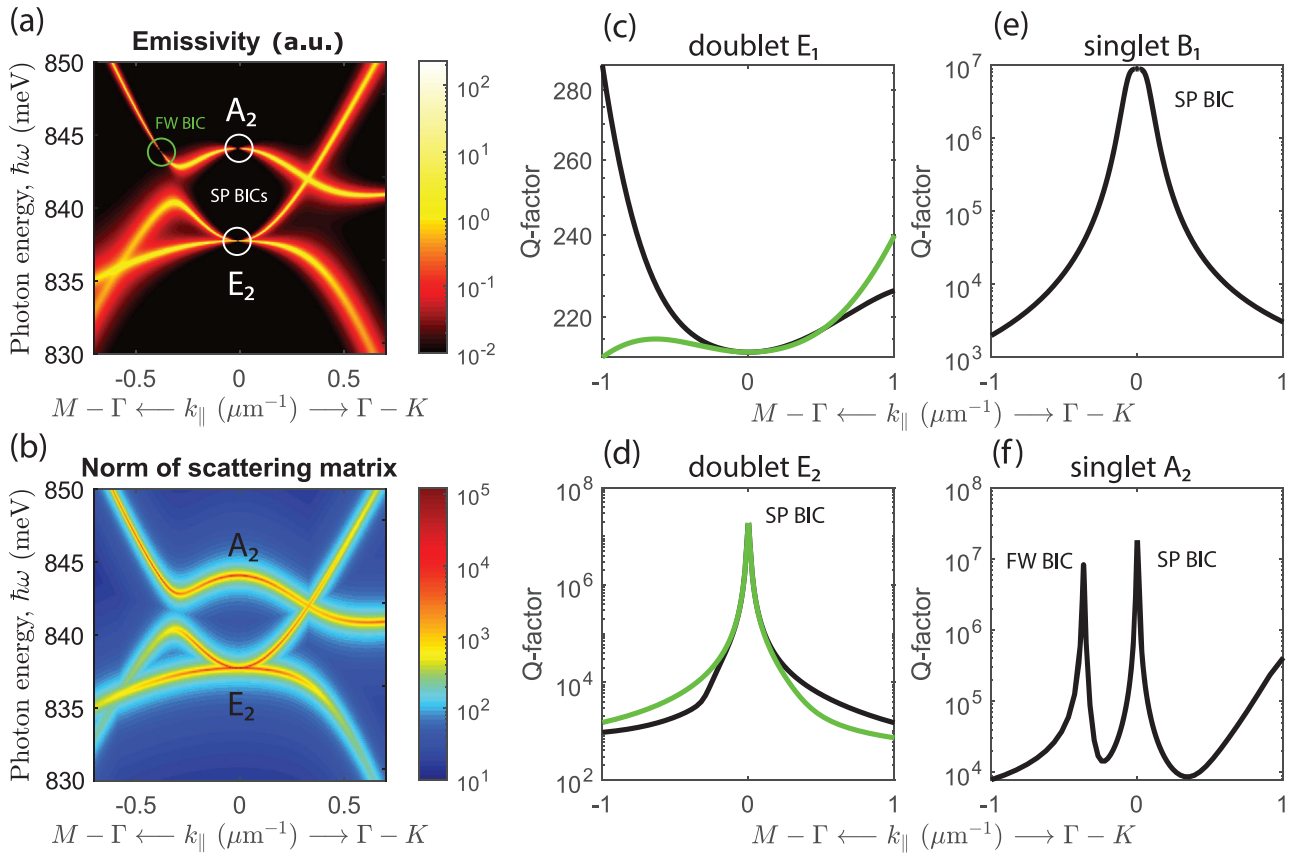

Figure 6. Calculated photon energy and wavevector dependence of a) emissivity and b) Frobenius norm of the scattering matrix near the Γ-point. Color scales are shown on the right. c–f) Calculated Q-factor of selected resonances near Γ-point. Calculation for panels (a–f) are made for $a = 600$ nm and $r/a = 0.2$ and effective refractive index of the layers with Ge nanoislands $n_{\text{eff}} = 3.12 + 10^{-6}i$. Symmetry-protected (SP) BIC and Friedrich–Wintgen (FW) BIC are highlighted.

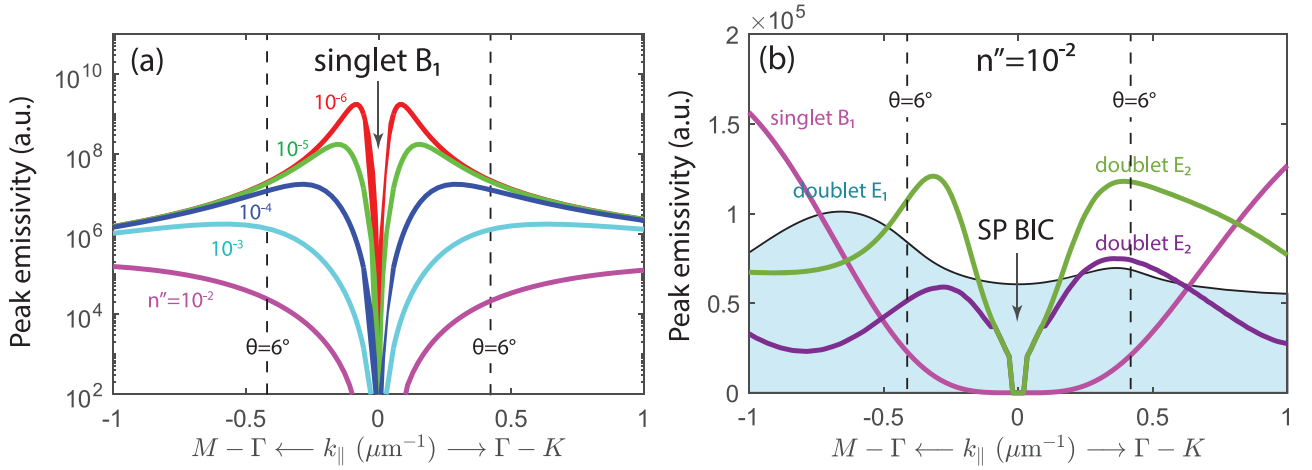

Figure 7. In-plane wavevector dependence of the peak emissivity calculated near a) the singlet B_1 for different imaginary parts of SiGe layer complex refractive index n'' and b) near the singlet B_1 and doublets E_1 and E_2 at $n'' = 10^{-2}$. Black dashed lines in (a) and (b) denote the 6° light cone at $\hbar\omega = 800$ meV. The curves for the two modes near the doublet E_1 are very similar in the displayed range of $k_{\|}$, so that only one of them is shown. Real part of the complex refractive index is fixed at $n' = 3.12$. The graphs in panels (a) and (b) should be interpreted in a manner that each point on a curve represents the photon energy where the emissivity reaches its maximum at certain value of $k_{\|}$. Note that the scale is logarithmic in (a) and linear in (b).

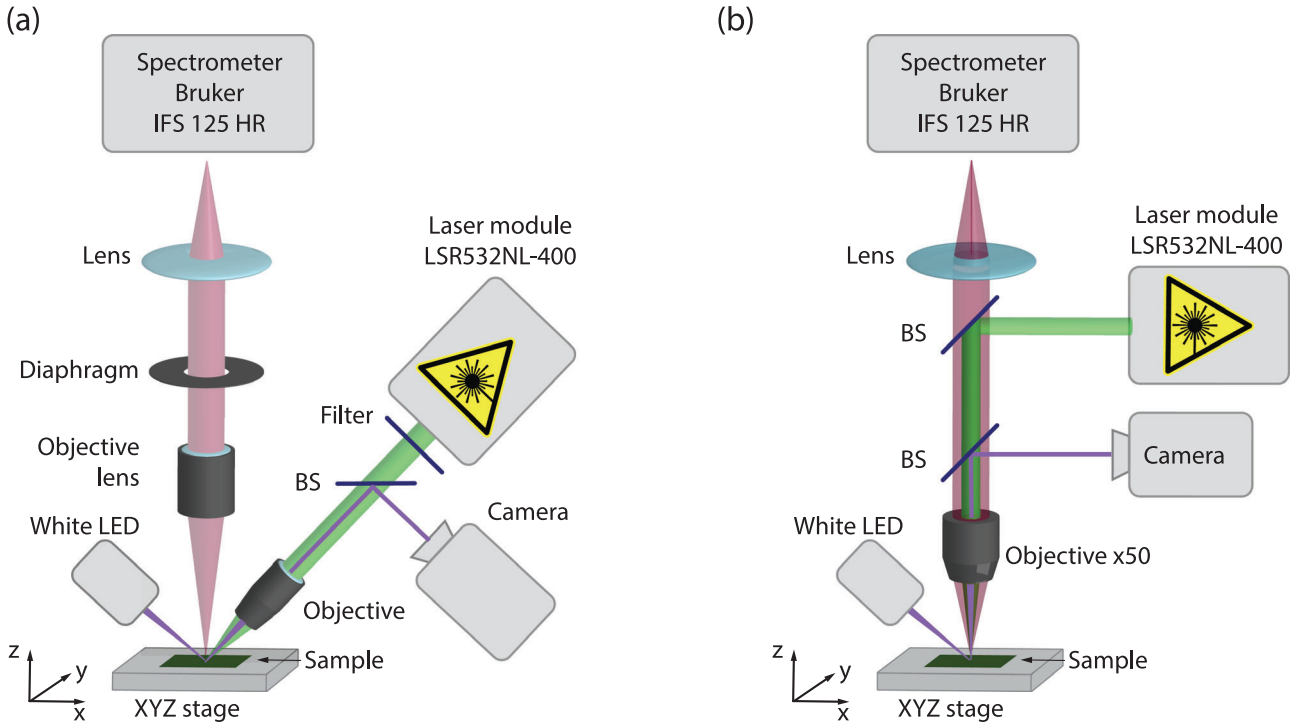

Figure 8. Schematics of a) the directional photoluminescence (DPL) setup and b) the microphotoliminescence (μPL) setup.

of singlet and doublet quasiguided modes in the Γ-point. We have classified these modes in terms of the group theory and have shown that in the C_{6v} symmetrical PCS, the doublet modes can be optically dark (E_2) and bright (E_1). We have associated the experimentally observed peaks to certain irreducible representations of C_{6v} point group. We also have shown that for the observation of BIC enhancement it is crucial to measure the photoluminescence response collecting the optical signal at angles close to normal. Finally, we have theoretically demonstrated the appearance of Friedrich–Wintgen BIC in our structure as a result of the destructive interference of two modes.

6. Experimental and Theoretical Methods

Sample Fabrication: Photonic crystals were formed on structures with self-assembled Ge nanoislands grown by molecular beam epitaxy. An SOI wafer from SOITEC company with a 3 μm thick oxide layer and a Si device layer thinned to 90 nm was used as a substrate. Grown structures consisted of a 75 nm thick Si buffer layer, 5 layers of Ge nanoislands separated by 15 nm thick Si spacer layers, and a 75 nm thick Si cap layer. The total thickness of the structure above the buried oxide was 300 nm. The islands were formed at 620 °C by the deposition of 7–8 monolayers of Ge. Under these growth conditions, an array of dome-shaped islands was formed on a silicon surface, with a surface density $\approx 10^{10}$ cm^{-2}, the lateral size of the islands of ≈70–80 nm, and the height before the overgrowth with the Si cap layer of ≈14–15 nm. The choice of the growth temperature was determined by the results of earlier studies demonstrating that the structures with dome-shaped Ge islands formed at around 600 °C provide the highest emission intensity at room temperature.[138] The luminescence properties of the "as grown" structures were analyzed in earlier works.[139]

PCSs were formed by electron-beam lithography and plasma-chemical etching. At the first step, a PCS's pattern was formed in a PMMA resist using electron-beam lithography. This pattern served as a mask during the etching of the structure. Anisotropic etching of PCSs was performed using ICP plasma-chemical etching in SF_6/C_4F_8 mixture of gases. In this work, PCSs with a hexagonal hole lattice were studied. The PCS lattice period, a, was varied in the range from 450 to 725 nm, and the ratio of the hole radius to the period, r/a, amounted to 0.2 and 0.26. The etching depth was 235 nm for $r/a = 0.2$ and 247 nm for $r/a = 0.26$. The overall size of the PCSs was 20×25 μm, thus PCSs contained more than 25×25 periods.

PL Measurements Setup: The light-emitting properties of PCSs were studied by applying two experimental techniques.

With the first technique, the luminescence response of the photonic crystal structures was measured with high spatial resolution. For this,a standard μPL setup (**Figure 8**a) was used, where the excitation light and the detecting signals through the same microscope objective were collected, which provided better spatial resolution. For the microscope objective with ×50 magnification (Mitutoyo M Plan APO objective, NA=0.42), the spatial resolution amounted to approximately 2 μm with the collection angles of up to ≈ 25° to normal.

To register the luminescence response at angles closer to the normal, a different setup was used, which was referred to as a DPL setup (Figure 8b). The PL signal was excited by a laser beam with 60° incidence. A Mitutoyo M Plan APO objective with ×10 magnification focused the laser beam on a spot with a diameter of ≈10 μm. The PL signal was collected by the Nikon 50 mm $f/1.4D$

AF Nikkor objective, which was located at the focal distance from the sample surface. In such a geometry, an emitted area can be considered as a point source. Accordingly, the light beam formed by the objective can be regarded as parallel. The parallelism of the light beam enabled one to use a diaphragm for collecting PL signals within small solid angles in the selected directions. PL measurements were conducted at the position of a diaphragm at the center of a parallel beam that corresponded to the maximal collection angle of ≈ 6° to normal.

All PL measurements were carried out at room temperature. The luminescence signal was excited by a solid-state CW laser emitting at the wavelength of 532 nm (laser module LSR532NL-400). To detect the PL signal, a high-resolution Fourier spectrometer (Bruker IFS 125 HR) and a nitrogen-cooled Ge photodetector were used. The spectral resolution in both experimental schemes can reach 0.05 cm^{-1}.

Theoretical Method: To theoretically study the optical behavior of the PCS with Ge nanoislands, a FMM in the scattering matrix form,[101] also known as rigorous coupled-wave analysis (RCWA)[140] was used. In the Fourier decomposition of electromagnetic fields, to preserve the C_{6v} symmetry of the structure, a C_6 symmetrical set of Fourier harmonics in the reciprocal space was chosen. The total number of harmonics was chosen to be $N_g = 199$ that ensured the convergence of our numerical scheme. As a result, the $4N_g \times 4N_g$ dimensional scattering matrix $\mathbf{S}(\omega, \vec{k}_\parallel)$ which contains full optical information of our photonic crystal slab was constructed. Here ω and $\vec{k}_\parallel$ denoted the frequency of electromagnetic oscillations and in-plane wavevector, respectively.

The photoluminescence of Ge nanoislands were modeled by the radiation of chaotically oriented oscillating electric dipoles which was a good approximation of emitting molecules or quantum dots. To calculate the emissivity spectra of oscillating dipoles, the electrodynamic reciprocity principle was used.[141] According to this principle the currents of two different dipoles $\vec{j}_{1,2}$ and their electric fields $\vec{E}_{1,2}$ at the positions of the other dipole were connected as $\vec{j}_1\vec{E}_2 = \vec{j}_2\vec{E}_1$. As a result, the problem of simulation of emissivity $I_i(\omega, \vec{k}_\parallel)$ of ith dipole at the frequency ω and wavevector $\vec{k}_\parallel$ was reduced to the calculation of the electric near field of a plane wave with the same ω and $\vec{k}_\parallel$ at the position of this dipole $\vec{r}_i$. The overall emissivity was found as a sum over the entire set of dipoles.

$$I(\omega, \vec{k}_\parallel) = \sum_i I_i(\omega, \vec{k}_\parallel) = \tag{5}$$

$$\sum_i |\vec{E}(\omega, \vec{k}_\parallel, \vec{r}_i)|^2 \tag{6}$$

where the subscript i denotes the ith dipole's current. The emission over the polarization states distributed randomly between the following polarization vectors was also averaged.

$$\vec{p}_1 = [1, 0] \tag{7}$$

$$\vec{p}_2 = [-1/2, -\sqrt{3}/2] \tag{8}$$

$$\vec{p}_3 = [-1/2, \sqrt{3}/2] \tag{9}$$

Such a set of polarization vectors preserved the C_{6v} rotational symmetry of the PCS.

Please note that in this work the emissivity rather than a full photoluminescence response was simulated. The latter should include a nonhomogeneous spatial excitation profile[142] which was omitted here as we focused here on explaining the nature and symmetry of the resonances.

The eigenmodes of the PCS were calculated by finding the poles of the scattering matrix.[143] The corresponding eigenvalue problem was be written as

$$\mathbf{S}^{-1}(\omega, \vec{k}_\parallel)\,|\mathbf{O}\rangle_{res} = |0\rangle \tag{10}$$

where, $|\mathbf{O}\rangle_{res}$ is the resonance output vector in the scattering matrix formalism (see Refs. [101, 143] for details). Problem (10) was solved by the generalized Newton's method by means of linearization of the inverse scattering matrix in the complex frequency domain.[143]

In FMM calculations, the layer with Ge nanoislands by an effective refractive index $n_{\text{eff}} = n' + n''i = 3.12{+}0.01\text{i}$ was described unless otherwise was stated. Dielectric permittivities of Si and SiO_2 were taken from Ref. [144]. In this work the convection $\exp(-i\omega t)$ for temporal dependencies of fields was used. In this convention, photon energies of eigenmodes had negative imaginary parts.

Character Table: To describe the symmetry of structure eigenmodes, the notations from the group theory where the symmetry is defined as a set of characters were used. For singlets, the characters are defined from

$$\hat{R}E_z = \chi(\hat{R})E_z \tag{11}$$

and for doublets

$$\hat{R}E_{1z} = \chi_{11}E_{1z} + \chi_{12}E_{2z} \tag{12}$$

$$\hat{R}E_{2z} = \chi_{21}E_{1z} + \chi_{22}E_{2z} \tag{13}$$

$$\chi(\hat{R}) = \chi_{11} + \chi_{22} \tag{14}$$

where $\hat{R}$ denotes a symmetry operation in a point group. The table of characters for C_{6v} point group is presented in Table 1.

Supporting Information

Supporting Information is available from the Wiley Online Library or from the author.

Acknowledgements

This work was supported in part by the Russian Science Foundation (project 19-72-10011). The theoretical analysis of the modes emissivity in Section 4 was supported by the Russian Science Foundation (project №16-12-10538П). S.A.D. acknowledges I. M. Fradkin for fruitful discussions. A.A.B. acknowledges the BASIS foundation and Grant of the President of the Russian Federation (MK-2224.2020.2).

Conflict of Interest

The authors declare no conflict of interest.

Data Availability Statement

The data that supports the findings of this study are available in the supporting information of this article.

Keywords

bound state in the continuum, germanium self-assembled quantum dot, photoluminescence enhancement, photonic crystal slab

Received: June 10, 2020
Revised: March 30, 2021
Published online:

[1] H. Ennen, J. Schneider, G. Pomrenke, A. Axmann, *Appl. Phys. Lett.* **1983**, *43*, 943.
[2] H. Ennen, G. Pomrenke, A. Axmann, K. Eisele, W. Haydl, J. Schneider, *Appl. Phys. Lett.* **1985**, *46*, 381.
[3] A. J. Kenyon, *Semicond. Sci. Technol.* **2005**, *20*, R65.
[4] Y. H. Xie, E. A. Fitzgerald, Y. J. Mii, *J. Appl. Phys.* **1991**, *70*, 3223.
[5] M. Q. Huda, S. I. Ali, *MRS Proc.* **2003**, *770*, I3.5.
[6] J. Liu, X. Sun, D. Pan, X. Wang, L. C. Kimerling, T. L. Koch, J. Michel, *Opt. Express* **2007**, *15*, 11272.
[7] J. Liu, X. Sun, R. Camacho-Aguilera, L. C. Kimerling, J. Michel, *Opt. Lett.* **2010**, *35*, 679.
[8] R. E. Camacho-Aguilera, Y. Cai, N. Patel, J. T. Bessette, M. Romagnoli, L. C. Kimerling, J. Michel, *Opt. Express* **2012**, *20*, 11316.
[9] S. Bao, D. Kim, C. Onwukaeme, S. Gupta, K. Saraswat, K. H. Lee, Y. Kim, D. Min, Y. Jung, H. Qiu, H. Wang, E. A. Fitzgerald, C. S. Tan, D. Nam, *Nat. Commun.* **2017**, *8*, 1.
[10] A. Elbaz, M. El Kurdi, A. Aassime, S. Sauvage, X. Checoury, I. Sagnes, C. Baudot, F. Boeuf, P. Boucaud, *APL Photonics* **2018**, *3*, 106102.
[11] F. A. Pilon, A. Lyasota, Y.-M. Niquet, V. Reboud, V. Calvo, N. Pauc, J. Widiez, C. Bonzon, J.-M. Hartmann, A. Chelnokov, J. Faist, H. Sigg, *Nat. Commun.* **2019**, *10*, 2724.
[12] G. Sun, *Opt. Quantum Electron.* **2012**, *44*, 563.
[13] R. Chen, S. Gupta, Y.-C. Huang, Y. Huo, C. W. Rudy, E. Sanchez, Y. Kim, T. I. Kamins, K. C. Saraswat, J. S. Harris, *Nano Lett.* **2014**, *14*, 37.
[14] S. Wirths, R. Geiger, N. von den Driesch, G. Mussler, T. Stoica, S. Mantl, Z. Ikonic, M. Luysberg, S. Chiussi, J.-M. Hartmann, H. Sigg, J. Faist, D. Buca, D. Grutzmacher, *Nat. Photonics* **2015**, *9*, 88.
[15] D. Stange, S. Wirths, R. Geiger, C. Schulte-Braucks, B. Marzban, N. von den Driesch, G. Mussler, T. Zabel, T. Stoica, J.-M. Hartmann, S. Mantl, Z. Ikonic, D. Grutzmacher, H. Sigg, J. Witzens, D. Buca, *ACS Photonics* **2016**, *3*, 1279.
[16] J. Chretien, N. Pauc, F. Armand Pilon, M. Bertrand, Q.-M. Thai, L. Casiez, N. Bernier, H. Dansas, P. Gergaud, E. Delamadeleine, R. Khazaka, H. Sigg, J. Faist, A. Chelnokov, V. Reboud, J.-M. Hartmann, V. Calvo, *ACS Photonics* **2019**, *6*, 2462.
[17] A. Elbaz, D. Buca, N. von den Driesch, K. Pantzas, G. Patriarche, N. Zerounian, E. Herth, X. Checoury, S. Sauvage, I. Sagnes, A. Foti, R. Ossikovski, J. Hartmann, F, Boeuf, Z. Ikonic, P. Boucad, D. Grutzmacher, M. El Kurdi, *Nat. Photonics* **2020**, *14*, 375.
[18] N. Koshida, H. Koyama, *Appl. Phys. Lett.* **1992**, *60*, 347.
[19] K. D. Hirschman, L. Tsybeskov, S. P. Duttagupta, P. M. Fauchet, *Nature* **1996**, *384*, 338.
[20] A. G. Cullis, L. T. Canham, *Nature* **1991**, *353*, 335.
[21] W. L. Wilson, P. Szajowski, L. Brus, *Science* **1993**, *262*, 1242.
[22] L. Pavesi, L. Dal Negro, C. Mazzoleni, G. Franzò, F. Priolo, *Nature* **2000**, *408*, 440.
[23] J. Valenta, M. Greben, S. Dyakov, N. Gippius, D. Hiller, S. Gutsch, M. Zacharias, *Sci. Rep.* **2019**, *9*, 1.
[24] S. A. Dyakov, D. M. Zhigunov, A. Marinins, M. R. Shcherbakov, A. A. Fedyanin, A. S. Vorontsov, P. K. Kashkarov, S. Popov, M. Qiu, M. Zacharias, S. G. Tikhodeev, N. A. Gippius, *Phys. Rev. B* **2016**, *93*, 205413.
[25] G. Dehlinger, L. Diehl, U. Gennser, H. Sigg, J. Faist, K. Ensslin, D. Grützmacher, E. Müller, *Science* **2000**, *290*, 2277.
[26] Y. B. Bolkhovityanov, O. P. Pchelyakov, *Phys.-Usp.* **2008**, *51*, 437.
[27] Q. Li, K. M. Lau, *Prog. Cryst. Growth Charact. Mater.* **2017**, *63*, 105.
[28] A. Y. Liu, J. Bowers, *IEEE J. Sel. Top. Quantum Electron.* **2018**, *24*, 1.
[29] J. C. Norman, D. Jung, Z. Zhang, Y. Wan, S. Liu, C. Shang, R. W. Herrick, W. W. Chow, A. C. Gossard, J. E. Bowers, *IEEE J. Quantum Electron.* **2019**, *55*, 1.
[30] A. W. Fang, H. Park, Y.-h. Kuo, R. Jones, O. Cohen, D. Liang, O. Raday, M. N. Sysak, M. J. Paniccia, J. E. Bowers, *Mater. Today* **2007**, *10*, 28.
[31] G. Roelkens, J. Van Campenhout, J. Brouckaert, D. Van Thourhout, R. Baets, P. R. Romeo, P. Regreny, A. Kazmierczak, C. Seassal, X. Letartre, Hollinger, J. M. Fedeli, L. Di Cioccio, C. Lagahe-Blanchard, *Mater. Today* **2007**, *10*, 36.
[32] H. Park, M. N. Sysak, H.-W. Chen, A. W. Fang, D. Liang, L. Liao, B. R. Koch, J. Bovington, Y. Tang, K. Wong, M. Jacob-Mitos, R. Jones, J. E. Bowers, *IEEE J. Sel. Top. Quantum Electron.* **2011**, *17*, 671.
[33] V. Y. Aleshkin, N. Bekin, N. Kalugin, Z. Krasil'nik, A. Novikov, V. Postnikov, H. Seyringer, *J. Exp. Theor. Phys. Lett.* **1998**, *67*, 48.
[34] V. G. Talalaev, G. E. Cirlin, A. A. Tonkikh, N. D. Zakharov, P. Werner, U. Gösele, J. W. Tomm, T. Elsaesser, *Nanoscale Res. Lett.* **2006**, *1*, 137.
[35] M. Grydlik, F. Hackl, H. Groiss, M. Glaser, A. Halilovic, T. Fromherz, W. Jantsch, F. Schäffler, M. Brehm, *ACS Photonics* **2016**, *3*, 298.
[36] V. Rutckaia, F. Heyroth, A. Novikov, M. Shaleev, M. Petrov, J. Schilling, *Nano Lett.* **2017**, *17*, 6886.
[37] S. David, M. El Kurdi, P. Boucaud, C. Kammerer, X. Li, S. Sauvage, V. Le Thanh, I. Sagnes, D. Bouchier, J.-M. Lourtioz, *Proc. SPIE 5450, Photonic Cryst. Mater. Nanostructures*, **2004**, p. 369, https://doi.org/10.1117/12.546572
[38] M. V. Stepikhova, A. V. Novikov, A. N. Yablonskiy, M. V. Shaleev, D. E. Utkin, V. V. Rutckaia, E. V. Skorokhodov, S. M. Sergeev, D. V. Yurasov, Z. F. Krasilnik, *Semicond. Sci. Technol.* **2019**, *34*, 2.
[39] C. Zeng, X. Hu, M. Shi, X. Qiu, Y. Li, J. Xia, *J. Light. Technol.* **2016**, *34*, 3283.
[40] S. Yuan, X. Qiu, C. Cui, L. Zhu, Y. Wang, Y. Li, J. Song, Q. Huang, J. Xia, *ACS Nano* **2017**, *11*, 10704.
[41] M. Schatzl, F. Hackl, M. Glaser, P. Rauter, M. Brehm, L. Spindlberger, A. Simbula, M. Galli, T. Fromherz, F. Schäffler, *ACS Photonics* **2017**, *4*, 665.
[42] Q. Quan, M. Loncar, *Opt. Express* **2011**, *19*, 18529.
[43] T. Yoshie, A. Scherer, J. Hendrickson, G. Khitrova, H. M. Gibbs, G. Rupper, C. Ell, O. B. Shchekin, D. G. Deppe, *Nature* **2004**, *432*, 200.
[44] P. Paddon, J. F. Young, *Phys. Rev. B* **2000**, *61*, 2090.
[45] C. W. Hsu, B. Zhen, A. D. Stone, J. D. Joannopoulos, M. Soljačić, *Nat. Rev. Mater.* **2016**, *1*, 16048.
[46] B. Zhen, C. W. Hsu, L. Lu, A. D. Stone, M. Soljačić, *Phys. Rev. Lett.* **2014**, *113*, 257401.
[47] M. Rybin, Y. Kivshar, *Nature* **2017**, *541*, 164.
[48] K. Koshelev, Y. Kivshar, *Nature* **2019**, *574*, 491.
[49] J. Jin, X. Yin, L. Ni, M. Soljačić, B. Zhen, C. Peng, *Nature* **2019**, *574*, 501.
[50] K. Koshelev, A. Bogdanov, Y. Kivshar, *Sci. Bull.* **2019**, *64*, 836
[51] M. Minkov, I. A. D. Williamson, M. Xiao, S. Fan, *Phys. Rev. Lett.* **2018**, *121*, 263901.
[52] T. Yoda, M. Notomi, arXiv:2004.09891, **2020**.
[53] M. Minkov, D. Gerace, S. Fan, *Optica* **2019**, *6*, 1039.

[54] A. C. Overvig, S. C. Malek, M. J. Carter, S. Shrestha, N. Yu, *Phys. Rev. B* **2020**, *102*, 035434.
[55] J. Wang, M. Clementi, M. Minkov, A. Barone, J.-F. Carlin, N. Grandjean, D. Gerace, S. Fan, M. Galli, R. Houdré, arXiv:2005.10355, **2020**.
[56] R. Gansch, S. Kalchmair, P. Genevet, T. Zederbauer, H. Detz, A. M. Andrews, W. Schrenk, F. Capasso, M. Lončar, G. Strasser, *Light: Sci. Appl.* **2016**, *5*, e16147.
[57] E. Tiguntseva, Z. Sadrieva, B. Stroganov, Y. V. Kapitonov, F. Komissarenko, R. Haroldson, B. Balachandran, W. Hu, Q. Gu, A. Zakhidov, A. Bogdanov, S. V. Makarov, *Appl. Surf. Sci.* **2019**, *473*, 419.
[58] L. Zhu, S. Yuan, C. Zeng, J. Xia, *Adv. Opt. Mater.* **2020**, *8*, 1901830.
[59] S. Romano, G. Zito, S. Manago?, G. Calafiore, E. Penzo, S. Cabrini, A. C. De Luca, V. Mocella, *J. Phys. Chem. C* **2018**, *122*, 19738.
[60] C. W. Hsu, B. Zhen, A. D. Stone, J. D. Joannopoulos, M. Soljačić, *Nat. Rev. Mater.* **2016**, *1*, 1.
[61] Y. Yang, C. Peng, Y. Liang, Z. Li, S. Noda, *Phys. Rev. Lett.* **2014**, *113*, 037401.
[62] M. V. Gorkunov, A. A. Antonov, Y. S. Kivshar, *Phys . Rev, Lett.* **2020**, *125*, 093903.
[63] M. Zhang, X. Zhang, *Sci. Rep.* **2015**, *5*, 1.
[64] K. Koshelev, A. Bogdanov, Y. Kivshar, *Opt. Photonics News* **2020**, *31*, 38.
[65] K. Koshelev, G. Favraud, A. Bogdanov, Y. Kivshar, A. Fratalocchi, *Nanophotonics* **2019**, *8*, 725.
[66] Z. Sadrieva, K. Frizyuk, M. Petrov, Y. Kivshar, A. Bogdanov, *Phys. Rev. B* **2019**, *100*, 115303.
[67] C. W. Hsu, B. Zhen, J. Lee, S.-L. Chua, S. G. Johnson, J. D. Joannopoulos, M. Soljačić, *Nature* **2013**, *499*, 188.
[68] E. N. Bulgakov, A. F. Sadreev, *Phys. Rev. A* **2019**, *99*, 033851.
[69] E. N. Bulgakov, D. N. Maksimov, *Opt. express* **2017**, *25*, 14134.
[70] J. von Neumann, E. Wigner, *Phys. Z.* **1929**, *30*, 465.
[71] V. Pacradouni, W. J. Mandeville, A. R. Cowan, P. Paddon, J. F. Young, S. R. Johnson, *Phys. Rev. B* **2000**, *62*, 4204.
[72] P. Paddon, J. F. Young, *Phys. Rev. B* **2000**, *61*, 2090.
[73] D. C. Marinica, a. G. Borisov, S. V. Shabanov, *Phys. Rev. Lett.* **2008**, *100*, 183902.
[74] E. N. Bulgakov, A. F. Sadreev, *Phys. Rev. B* **2008**, *78*, 075105.
[75] V. Mocella, S. Romano, *Phys. Rev. B* **2015**, *92*, 155117.
[76] J. W. Yoon, S. H. Song, R. Magnusson, *Sci. Rep.* **2015**, *5*, 18301.
[77] A. Kodigala, T. Lepetit, Q. Gu, B. Bahari, Y. Fainman, B. Kanté, *Nature* **2017**, *541*, 196.
[78] B. Bahari, F. Vallini, T. Lepetit, R. Tellez-Limon, J. Park, A. Kodigala, Y. Fainman, B. Kante, **2017**, arXiv:1707.00181.
[79] S. T. Ha, Y. H. Fu, N. K. Emani, Z. Pan, R. M. Bakker, R. Paniagua-Domínguez, A. I. Kuznetsov, *Nat. Nanotechnol.* **2018**, *13*, 1042.
[80] J. M. Foley, S. M. Young, J. D. Phillips, *Phys. Rev. B* **2014**, *89*, 165111.
[81] X. Cui, H. Tian, Y. Du, G. Shi, Z. Zhou, *Sci. Rep.* **2016**, *6*, 36066.
[82] S. Romano, G. Zito, S. Torino, G. Calafiore, E. Penzo, G. Coppola, S. Cabrini, I. Rendina, V. Mocella, *Photonics Res.* **2018**, *6*, 726.
[83] S. Romano, A. Lamberti, M. Masullo, E. Penzo, S. Cabrini, I. Rendina, V. Mocella, *Materials* **2018**, *11*, 526.
[84] Y. Liu, W. Zhou, Y. Sun, *Sensors* **2017**, *17*, 1861.
[85] V. Kravtsov, E. Khestanova, F. A. Benimetskiy, T. Ivanova, A. K. Samusev, I. S. Sinev, D. Pidgayko, A. M. Mozharov, I. S. Mukhin, M. S. Lozhkin, Y. V. Kapitonov, A. S. Brichkin, V. D. Kulakovskii, I. A. Shelykh, A. I. Tartakovskii, P. M. Walker, M. S. Skolnick, D. N. Krizhanovskii, I. V. Iorsh, *Light: Sci. Appl.* **2020**, *9*, 56.
[86] K. Koshelev, S. Sychev, Z. F. Sadrieva, A. A. Bogdanov, I. Iorsh, *Phys. Rev. B* **2018**, *98*, 161113.
[87] H. M. Doeleman, F. Monticone, W. den Hollander, A. Alù, A. F. Koenderink, *Nat. Photonics* **2018**, *12*, 397.
[88] Y. Zhang, A. Chen, W. Liu, C. W. Hsu, B. Wang, F. Guan, X. Liu, L. Shi, L. Lu, J. Zi, *Phys. Rev. Lett.* **2018**, *120*, 186103.
[89] K. Koshelev, Y. Tang, K. Li, D.-Y. Choi, G. Li, Y. Kivshar, *ACS Photonics* **2019**, *6*, 1639.
[90] S. Krasikov, A. Bogdanov, I. Iorsh, *Phys. Rev. B* **2018**, *97*, 224309.
[91] E. N. Bulgakov, D. N. Maksimov, *Sci. Rep.* **2019**, *9*, 1.
[92] E. Bulgakov, K. Pichugin, A. Sadreev, *Phys. Rev. B* **2011**, *83*, 045109.
[93] E. Bulgakov, K. Pichugin, A. Sadreev, *J .Phy.: Condens. Matter* **2013**, *25*, 395304.
[94] M. V. Rybin, K. L. Koshelev, Z. F. Sadrieva, K. B. Samusev, A. A. Bogdanov, M. F. Limonov, Y. S. Kivshar, *Phys. Rev. Lett.* **2017**, *119*, 243901.
[95] K. Koshelev, S. Kruk, E. Melik-Gaykazyan, J.-H. Choi, A. Bogdanov, H.-G. Park, Y. Kivshar, *Science* **2020**, *367*, 288.
[96] V. Mylnikov, S. T. Ha, Z. Pan, V. Valuckas, R. Paniagua-Dominguez, H. V. Demir, A. I. Kuznetsov, arXiv:2003.03922, **2020**.
[97] A. A. Bogdanov, K. L. Koshelev, P. V. Kapitanova, M. V. Rybin, S. A. Gladyshev, Z. F. Sadrieva, K. B. Samusev, Y. S. Kivshar, M. F. Limonov, *Adv. Photonics* **2019**, *1*, 016001.
[98] T. Asano, Y. Ochi, Y. Takahashi, K. Kishimoto, S. Noda, *Opt. Express* **2017**, *25*, 1769.
[99] S. L. Portalupi, M. Galli, C. Reardon, T. Krauss, L. O'Faolain, L. C. Andreani, D. Gerace, *Opt. Express* **2010**, *18*, 16064.
[100] C. Dineen, J. Förstner, A. Zakharian, J. V. Moloney, S. W. Koch, *Opt. Express* **2005**, *13*, 4980.
[101] S. G. Tikhodeev, A. L. Yablonskii, E. A. Muljarov, N. A. Gippius, T. Ishihara, *Phys. Rev. B* **2002**, *66*, 045102.
[102] S. Fan, J. D. Joannopoulos, *Phys. Rev. B* **2002**, *65*, 235112.
[103] A. Gras, W. Yan, P. Lalanne, arXiv:1905.12359, **2019**.
[104] P. Lalanne, W. Yan, A. Gras, C. Sauvan, J.-P. Hugonin, M. Besbes, G. Demésy, M. D. Truong, B. Gralak, F. Zolla, A. Nicolet, F. Binkowski, L. Zschiedrich, S. Burger, J. Zimmerling, R. Remis, P. Urbach, H. T. Liu, T. Weiss, *J. Opt. Soc. Am. A* **2019**, *36*, 686.
[105] M. Wu, S. T. Ha, S. Shendre, E. G. Durmusoglu, W.-K. Koh, D. R. Abujetas, J. A. Sánchez-Gil, R. Paniagua-Dominguez, H. V. Demir, A. I. Kuznetsov, *Nano Lett.* **2020**, *20*, 6005.
[106] K. Fan, I. V. Shadrivov, W. J. Padilla, *Optica* **2019**, *6*, 169.
[107] W. Liu, B. Wang, Y. Zhang, J. Wang, M. Zhao, F. Guan, X. Liu, L. Shi, J. Zi, *Phys. Rev. Lett.* **2019**, *123*, 116104.
[108] Y. Liang, K. Koshelev, F. Zhang, H. Lin, S. Lin, J. Wu, B. Jia, Y. Kivshar, *Nano Lett.* **2020**, *20*, 6351.
[109] S. Han, L. Cong, Y. K. Srivastava, B. Qiang, M. V. Rybin, A. Kumar, R. Jain, W. X. Lim, V. G. Achanta, S. S. Prabhu, Q. J. Wang, Y. S. Kivshar, R. Singh, *Adv. Mater.* **2019**, *31*, 1901921.
[110] T. G. Nguyen, G. Ren, S. Schoenhardt, M. Knoerzer, A. Boes, A. Mitchell, *Laser Photonics Rev.* **2019**, *13*, 1900035.
[111] M. Liu, D.-Y. Choi, *Nano Lett.* **2018**, *18*, 8062.
[112] D. R. Abujetas, N. van Hoof, S. ter Huurne, J. G. Rivas, J. A. Sánchez-Gil, *Optica* **2019**, *6*, 996.
[113] G. Zito, S. Romano, S. Cabrini, G. Calafiore, A. C. De Luca, E. Penzo, V. Mocella, *Optica* **2019**, *6*, 1305.
[114] Y. K. Srivastava, R. T. Ako, M. Gupta, M. Bhaskaran, S. Sriram, R. Singh, *Appl. Phys. Lett.* **2019**, *115*, 151105.
[115] S. Murai, D. R. Abujetas, G. W. Castellanos, J. A. Sanchez-Gil, F. Zhang, J. G. Rivas, *ACS Photonics* **2020**, *7*, 2204.
[116] N. Karl, P. P. Vabishchevich, S. Liu, M. B. Sinclair, G. A. Keeler, G. M. Peake, I. Brener, *Appl. Phys. Lett.* **2019**, *115*, 141103.
[117] T. C. Tan, E. Plum, R. Singh, *Adv. Opt. Mater.* **2020**, *8*, 6.
[118] Z. Liu, Y. Xu, Y. Lin, J. Xiang, T. Feng, Q. Cao, J. Li, S. Lan, J. Liu, *Phys. Rev. Lett.* **2019**, *123*, 253901.
[119] F. Yesilkoy, E. R. Arvelo, Y. Jahani, M. Liu, A. Tittl, V. Cevher, Y. Kivshar, H. Altug, *Nat. Photonics* **2019**, *13*, 390.
[120] A. Tittl, A. Leitis, M. Liu, F. Yesilkoy, D.-Y. Choi, D. N. Neshev, Y. S. Kivshar, H. Altug, *Science* **2018**, *360*, 1105.
[121] H. Liu, C. Guo, G. Vampa, J. L. Zhang, T. Sarmiento, M. Xiao, P. H. Bucksbaum, J. Vučković, S. Fan, D. A. Reis, *Nat. Phys* **2018**, *14*, 1006.

[122] C. Cui, C. Zhou, S. Yuan, X. Qiu, L. Zhu, Y. Wang, Y. Li, J. Song, Q. Huang, Y. Wang, C. Zeng, J. Xia, *ACS Photonics* **2018**, *5*, 4074.
[123] S. Campione, S. Liu, L. I. Basilio, L. K. Warne, W. L. Langston, T. S. Luk, J. R. Wendt, J. L. Reno, G. A. Keeler, I. Brener, M. B. Sinclair, *Acs Photonics* **2016**, *3*, 2362.
[124] Y. Yang, I. I. Kravchenko, D. P. Briggs, J. Valentine, *Nat. Commun.* **2014**, *5*, 1.
[125] A. Kodigala, T. Lepetit, Q. Gu, B. Bahari, Y. Fainman, B. Kanté, *Nature* **2017**, *541*, 196.
[126] S. Yuan, X. Qiu, C. Cui, L. Zhu, Y. Wang, Y. Li, J. Song, Q. Huang, J. Xia, *ACS Nano* **2017**, *11*, 10704.
[127] S. Romano, M. Mangini, E. Penzo, S. Cabrini, A. C. De Luca, I. Rendina, V. Mocella, G. Zito, *ACS Nano* **2020**, *14*, 15417.
[128] B. Wang, W. Liu, M. Zhao, J. Wang, Y. Zhang, A. Chen, F. Guan, X. Liu, L. Shi, J. Zi, *Nat. Photonics* **2020**, *14*, 623.
[129] K. Sakoda, *Opt. Exp.* **2012**, *20*, 25181.
[130] K. Sakoda, *Optical Properties of Photonic Crystals*, Springer, Berlin**2001**.
[131] J. Zhu, Ş. K. Özdemir, H. Yilmaz, B. Peng, M. Dong, M. Tomes, T. Carmon, L. Yang, *Sci. Rep.* **2014**, *4*, 1.
[132] Q. Zhang, H. Yu, M. Barbiero, B. Wang, M. Gu, *Light: Sci. Appl.* **2019**, *8*, 1.
[133] S. A. Dyakov, V. A. Semenenko, N. A. Gippius, S. G. Tikhodeev, *Phys. Rev. B* **2018**, *98*, 235416.
[134] D. Marinica, A. Borisov, S. Shabanov, *Phys. Rev. Lett.* **2008**, *100*, 183902.
[135] H. Friedrich, D. Wintgen, *Phys. Rev. A* **1985**, *32*, 3231.
[136] S. Gladyshev, A. Bogdanov, P. Kapitanova, M. Rybin, K. Koshelev, Z. Sadrieva, K. Samusev, Y. Kivshar, M. Limonov, In *Journal of Physics: Conference Series* (Ed.: A. Ashton), volume 1124. IOP Publishing, Bristol **2018**, p. 051058.
[137] S. Dyakov, E. Astrova, T. Perova, S. Tikhodeev, N. Gippius, V. Y. Timoshenko, *J. Exp. Theoretical Phys.* **2011**, *113*, 80.
[138] N. V. Vostokov, Y. N. Drozdov, Z. F. Krasilnik, D. Lobanov, A. V. Novikov, A. N. Yablonskii, *J. Exp. Theor. Phys. Lett.* **2002**, *76*, 365.
[139] Z. Krasilnik, A. Novikov, D. Lobanov, K. Kudryavtsev, A. Antonov, S. Obolenskiy, N. Zakharov, P. Werner, *Semicond. Sci. Technol.* **2010**, *26*, 014029.
[140] M. Moharam, T. Gaylord, E. B. Grann, D. A. Pommet, *JOSA a* **1995**, *12*, 1068.
[141] S. V. Lobanov, S. G. Tikhodeev, N. A. Gippius, A. A. Maksimov, E. V. Filatov, I. I. Tartakovskii, V. D. Kulakovskii, T. Weiss, C. Schneider, J. Gessler, M. Kamp, S. Hoefling, *Phys. Rev. B* **2015**, *92*, 205309.
[142] S. A. Dyakov, D. M. Zhigunov, A. Marinins, O. A. Shalygina, P. P. Vabishchevich, M. R. Shcherbakov, D. E. Presnov, A. A. Fedyanin, P. K. Kashkarov, S. Popov, N. A. Gippuius, S. G. Tikhodeev, *Sci. Rep.* **2018**, *8*, 4911.
[143] N. A. Gippius, S. G. Tikhodeev, T. Ishihara, *Phys. Rev. B* **2005**, *72*, 045138.
[144] E. D. Palik, G. Ghosh, *Handbook of Optical Constants of Solids*, Vol. 3, Academic Press, Cambridge **1998**.